Since January 2020 Elsevier has created a COVID-19 resource centre with free information in English and Mandarin on the novel coronavirus COVID-19. The COVID-19 resource centre is hosted on Elsevier Connect, the company's public news and information website.

Bioelectrochemistry 142 (2021) 107894

Contents lists available at ScienceDirect

Bioelectrochemistry

journal homepage: www.elsevier.com/locate/bioelechem

Responses of electroactive biofilms to chronic chlorine exposure: Insights from the composition and spatial structure of extracellular polymeric substances

Yue Dong [a], Mingrui Sui [b,*], Xin Wang [c], Peng Zhang [d], Yiying Jiang [a], Jianyu Wu [a]

[a] Key Laboratory of Integrated Regulation and Resource Development on Shallow Lakes of Ministry of Education, College of Environment, Hohai University, Nanjing 210098, China
[b] College of Water Conservancy and Hydropower Engineering, Hohai University, Nanjing 210098, China
[c] MOE Key Laboratory of Pollution Processes and Environmental Criteria and Tianjin Key Laboratory of Environmental Remediation and Pollution Control, College of Environmental Science and Engineering, Nankai University, Tianjin 300350, China
[d] Faculty of Environmental Science and Engineering, Kunming University of Science and Technology, Kunming 650500, China

ARTICLE INFO

Article history:
Received 9 May 2021
Received in revised form 20 July 2021
Accepted 21 July 2021
Available online 27 July 2021

Keywords:
Electroactive biofilms (EABs)
Chronic chlorine exposure
Extracellular polymeric substances (EPS)
Pollutant degradation
Electron exchange capacities

ABSTRACT

Extensive amounts of chlorine disinfectants have been applied to wastewater system since the outbreak of coronavirus disease 2019 (COVID-19), which inevitably affects the pollutant degradation via interfering with electron transfer mediated by electroactive bacteria. Herein, the response of electroactive biofilm (EAB) to chronic chlorine exposure was investigated. Results showed the EAB formed without exposure (EAB-0) exhibited a 53% and 123% higher current output than that formed with 0.1 mg L^{-1} (EAB-0.1) and 0.5 mg L^{-1} (EAB-0.5) chlorine, respectively. The chronic chlorine exposure of EAB boosted the contents of extracellular polymeric substances (EPS) in EAB-0.1 and EAB-0.5 by over secretion of extracellular polysaccharides. The EAB-0.1 and EAB-0.5 also presented lower electron exchange capacities (EECs) of EPS, coincided with reduced relative abundance of *Geobacter* from 61% in EAB-0 to 52% in EAB-0.5. This study provided new insights into the application of engineered EAB for wastewater treatment in a disinfection environment.

1. Introduction

Chlorine disinfectants are widely used for wastewater and drinking water disinfection due to its low cost and complete inactivation of pathogenic microorganisms [1]. In recent efforts to contain the spread of the coronavirus disease 2019 (COVID-19), extensive amounts of chlorine disinfectants were applied to both public and domestic spaces [2,3]. Inevitably, this residual chlorine will eventually be released into wastewater treatment systems, putting the biological treatment process at risk.

Electroactive biofilm (EAB), as the most important part of bioelectrochemical system (BES), is capable of regulating the pollutant removal and reducing energy consumption for wastewater treatment [4]. When using engineered EAB in real world applications, the effect of chronic chlorine exposure on its performance must be considered. Residual chlorine is both direct and effective in significantly reducing viable cell numbers and inhibiting cell activity [5]. The stimulation of residual chlorine can also impose selective pressure on the formation and maintenance of the EAB spatial structure to resist chlorine toxicity. Numerous studies have demonstrated the deteriorative electroactivity following the interaction between EABs and toxic substances, with lower pollutant degradation efficiency [6,7]. However, research correlating the electroactivity of EAB when exposed to chlorine, as well as the impact of this correlation on the pollutant degradation performance, is limited.

Proteins and polysaccharides act as the dominant components in EPS, playing an important role in shaping the EAB spatial structure [8]. In particular, the protein components of EPS can assist in the formation of conductive networks for EAB [9,10]. A strong response relationship has been detected between current and redox-active protein content in well-cultivated EABs, namely, a limited current output corresponding to a low protein content because the electron transfer was closely associated with the outer membrane and extracellular redox-active proteins in the region closer to electrode [11]. In contrast, polysaccharides, as insulative components, impose an adverse impact on electron transfer by isolating the conductive proteins trapped therein. But, they are still considered as indispensable to EABs as both main biofilm skeleton

* Corresponding author.
E-mail address: suimingruihit@163.com (M. Sui).

https://doi.org/10.1016/j.bioelechem.2021.107894
1567-5394/

and protective barrier, thus greatly affecting electron transfer [12]. How does chlorine exposure affect the proteins and polysaccharides contents? Does the componential variation affect EAB performance? The answers of these questions were important to elucidate the mechanisms and impacts of chronic chlorine exposure on EAB performance.

In this study, the EABs were cultivated at chlorine concentrations of 0, 0.1 and 0.5 mg L^{-1}. The objectives of this study are: (1) to explore the impact of chronic chlorine exposure on the electrochemical behavior of EAB; (2) to gain a comprehensive insight into the variations in production and spatial distribution characteristics of EPS conditioned with chlorine; (3) to further explore the potential mechanism of chronic chlorine exposure on variations of microbial composition and electron transfer capacity of EPS.

2. Materials and methods

2.1. Construction and operation of the BES

The BESs were constructed using transparent plexiglass of the same cross-sectional dimensions (Length: 5 × Height: 12 cm). Furthermore, the anode and cathode chambers had a thickness of 4 cm. The two chambers were clamped together with gaskets and separated using a cation exchange membrane (CEM, Ultrex CMI7000, Membranes International). The anode contained two parallel carbon fiber brushes (L: 10 × Φ: 2 cm, 3 K carbon fiber, Toray). The brushes were pretreated in a muffle furnace at 450 °C for 30 min before use [13]. A graphite sheet (Length: 4 × Height: 10 × Thickness: 1 cm) was used as cathode. The working volumes of the anode and cathode chambers were 195 mL and 200 mL, respectively.

The BES was inoculated by the effluent of a long-term operated microbial fuel cell (20%, v/v) and fed with anhydrous sodium acetate (1 g L^{-1}). The medium contained a 50 mM phosphate buffer solution (PBS, Na_2HPO_4, 4.576 g L^{-1}; NaH_2PO_4, 2.132 g L^{-1}; NH_4Cl, 0.31 g L^{-1}; KCl, 0.13 g L^{-1}), a 5 mL L^{-1} vitamin solution and a 12.5 mL L^{-1} trace mineral solution [14]. The chlorine exposure was performed by dissolving Clorox bleach (Bozhi Co., Jinan, China) in the medium with chlorine concentrations of 0 (control), 0.1 and 0.5 mg L^{-1}. The chlorine concentrations were set based on the preferred disinfectants of chloramine and chlorine dioxide disinfectant for city water supplies in China (GB5749-2006) (Table S1). Note that the chlorine concentration was the sole parameter controlling the BES operation. The cathode chamber contained potassium ferricyanide (50 mM $K_3[Fe(CN)_6]$ and 50 mM KCl). Corresponding BESs were marked as BES-0, BES-0.1 and BES-0.5, with the EABs of EAB-0, EAB-0.1 and EAB-0.5. All tests were repeated in triplicate and operated in batch mode with the medium replaced at the end of each cycle.

2.2. Electrochemical characterizations

The external resistance (R) for all BESs was set as 100 Ω. The voltages (U) were recorded every 30 min using a PISO-813 data acquisition system (ICP DAS Co., Ltd.).The current (I) was calculated via the formula $I = U/R$. The current data was reported based on the average of the triplicate reactors. The current conversion efficiency was calculated based on COD removal according to previous research [7]. The electroactivity of the enriched EABs was examined by cyclic voltammetry (CV) under both turnover condition with acetate (1 g L^{-1}) and non-turnover condition without the substrate. CV analysis of EAB was performed in a three-electrode system with the anode as working electrode, the graphite sheet as counter electrode, and an Ag/AgCl electrode as reference electrode (+200 mV vs SHE) using a workstation (Autolab PGSTAT128N, Metrohm Co., Swiss). The turnover CV testing was performed between −0.6 and 0.4 V at a scan rate of 1 mV s^{-1}. Non-turnover CV tests with various scan rates of 1, 5, 20, 50 and 100 mV s^{-1} were conducted in order to identify the principle technique of electron transfer between the EAB and electrode. All CV tests were repeated three times, with the third observations employed for the consequent analysis. The EPS was extracted from the EABs using previously reported methods [15]. The electron transfer capacities of the EPS were established by determining their electron accepting capacity (EAC) mediated by the electrochemical reduction (MER) method, and electron donating capacity (EDC) mediated by the electrochemical oxidation (MEO) method [16]. The EPS amount was based on the sum of protein and polysaccharide contents.

The EAB biomass adhesion ratio (k_b) and protein adhesion ratio (k_p) were determined in order to evaluate the EAB characteristics. The volatile suspended solids (VSS) (m_v) of the EABs were measured according to a standard method [17]. The protein content (m_p) on the anode was measured via a BCA protein quantification assay kit (Solarbio, Beijing) [18]. Prior to the measurements, the biofilm was scraped from the electrode using sterile surgical scissors at 6 random sampling points (3 points for the VSS test and additional 3 points for the protein test). The remaining carbon fiber was then oven dried to the constant weight of m_c at 105 °C for 24 h. The biomass adhesion ratio and protein adhesion ratio were determined via the formulas $k_b = m_v/m_c$ and $k_p = m_p/m_c$, respectively. The biofilm electroactivity (mA g^{-1} protein) was calculated by normalizing the current (mA) to the measured protein content.

2.3. Spatial structure and composition of EPS

2.3.1. EPS spatial structure

The spatial distribution of EPS component in the EAB was visualized using multiple color staining technology and confocal laser scanning microscopy (CLSM) imaging [19]. The biofilm sample was randomly selected from the mixed carbon fibers at 3 points in the parallel BESs with the same chlorine concentration using sterile surgical scissors and placed on a slide. The biofilm sample was fixed with 2.5% glutaraldehyde for 12 h at 4 °C, followed by fluorescent staining via fluorescein-isothiocyanate (FITC) (Sigma, St. Louis, MO), concanavalin A (Con A) (Invitrogen Life Science, USA) and calcofluor white (CW) (Sigma, St. Louis, MO) to visualize the protein and α- and β-D-glucopyranose PS, respectively [20,21]. In particular, $NaHCO_3$ buffer (0.1 M) was added to the biofilm sample to retain the amine group in its non-protonated form [21]. Following this, 1 g L^{-1} FITC (dissolved in dimethylsulfoxide) was added and the solution was incubated at room temperature for 1 h. Thereafter, 0.25 g L^{-1} Con A (dissolved in 0.1 M $NaHCO_3$) solution was added for 30 min, followed by 0.3 g L^{-1} CW for an additional 30 min. Once the biofilm samples were stained, they were washed with 50 mM PBS to remove excess stains. Finally, the stained samples were observed through a CLSM (Nikon A1, Japan). FITC, Con A and CW were observed at the excitation/emission wavelengths of 488/520 (green), 561/580 (red) and 400/435 nm (blue), respectively [22].

Semi-quantitative analysis on the spatial distribution characteristics of protein and α- and β-D-glucopyranose PS was performed as follows. The original color two-dimensional images of each layer in the three-dimensional CLSM image were converted to gray images with pixel values between 0 (black) and 255 (white) in MATLAB® (MathWorks) [22]. The pixel value of each point (807 × 807) was subsequently extracted and used for analysis.

2.3.2. The composition analysis of EPS

The loose-bound EPS (LB-EPS) and tight-bound EPS (TB-EPS) were extracted using a previously reported method at the end of the experiments [23]. More specifically, the carbon fiber from a random carbon fiber brush of a BES reactor was cut using sterile

surgical scissors and sterile tweezers. The carbon fiber was then rinsed with deionized water to remove large flocs and placed in 50 mL centrifuge tubes to form 50 mL suspension via the NaCl solution (0.05%, w/w). The suspension was sonicated at 20 kHz for 2 min and horizontally vibrated at 150 rpm for 30 min. This was followed by centrifugation at 6000*g* for 20 min, with the resultant supernatant collected and denoted LB-EPS. The residual carbon fiber was then resuspended with NaCl solution to 50 mL, sonicated at 20 kHz for 2 min and subsequently heated at 60 °C for 30 min. The suspensions were centrifuged at 12,000*g* for 20 min and the supernatant was collected as the TB-EPSs. The LB-EPS and TB-EPS supernatants were filtered using a 0.45 μm filtration membrane and stored at 4 °C prior to analysis. Polysaccharide content was determined by the anthrone method [24], while protein content was measured via a BCA protein quantification assay kit (Solarbio, Beijing) [18]. The EPS component concentrations were expressed by normalizing the EPS concentration to the measured VSS content (mg g^{-1} VSS).

2.4. Pollutant removal, EAB community analysis and micromorphology observation

The chemical oxygen demand (COD) was measured following 2, 4, 8, 10, 12, 24, 36 and 48 h of operation based on the APHA standard method [25]. The average and standard deviation (±SD) of the COD concentration were calculated by duplicating the measurements. The EAB communities were analyzed using the high-throughput 16S rRNA genetic clone library. Three parallel samples from 3 random points on one carbon fiber brush were merged into one sample. The variable region V3-V4 of bacterial 16S rRNA was amplified with the forward primer 341F (5′-CCTACGGGNGGCWGCAG-3′) and reverse primer 805R (5′-GACTACHVGGGTATCTAATCC-3′). The pyrosequencing of the amplicons was performed by Sangon Biotech Company (Shanghai, China). Sequences were clustered into operational taxonomic units (OTUs) based on a minimum similarity of 97% [26]. The micromorphology of the EAB was observed using a field-emission scanning electron microscope (SEM, FEI Quanta 200F). Prior to imaging, an electronically conductive Au coating was applied to each EAB sample to reduce charging in the SEM.

2.5. Calculations and statistical analysis

The distribution of proteins and polysaccharides in EAB was fitted using the exponentially modified Gaussian (EMG) model as follows [27].

$$f_1(x) = \frac{A}{t_0} e^{-\frac{x}{t_0}} \tag{1}$$

$$f_2(x) = \frac{1}{w\sqrt{2\pi}} e^{-\frac{(x-x_c)^2}{2w^2}} \tag{2}$$

$$z = \frac{x - x_c}{w} - \frac{w}{t_0} \tag{3}$$

$$f(x) = y_0 + (f_1 \times f_2)(x) = y_0 + \frac{A}{t_0} e^{\frac{1}{2}\left(\frac{w}{t_0}\right)^2 - \frac{x-x_c}{t_0}} \int_{-\infty}^{z} \frac{1}{\sqrt{2\pi}} e^{-\frac{y^2}{2}} dy \tag{4}$$

where y_0 is the offset, A is the area of the curve, x_c and w are the center and width of the biofilm sample, t_0 is the time constant of the exponential modifier.

All measurements were conducted in triplicate and reported as the mean ± SD based on the 3 parallel BESs with the same chlorine concentration. The SPSS (22.0, IBM) was used for the correlation analysis of EPS contents, electrochemical parameters and COD degradation efficiency.

3. Results and discussion

3.1. EAB electroactivity

A gradual increase in the current was observed in BES-0, BES-0.1 and BES-0.5 during the 90 days of operation, demonstrating

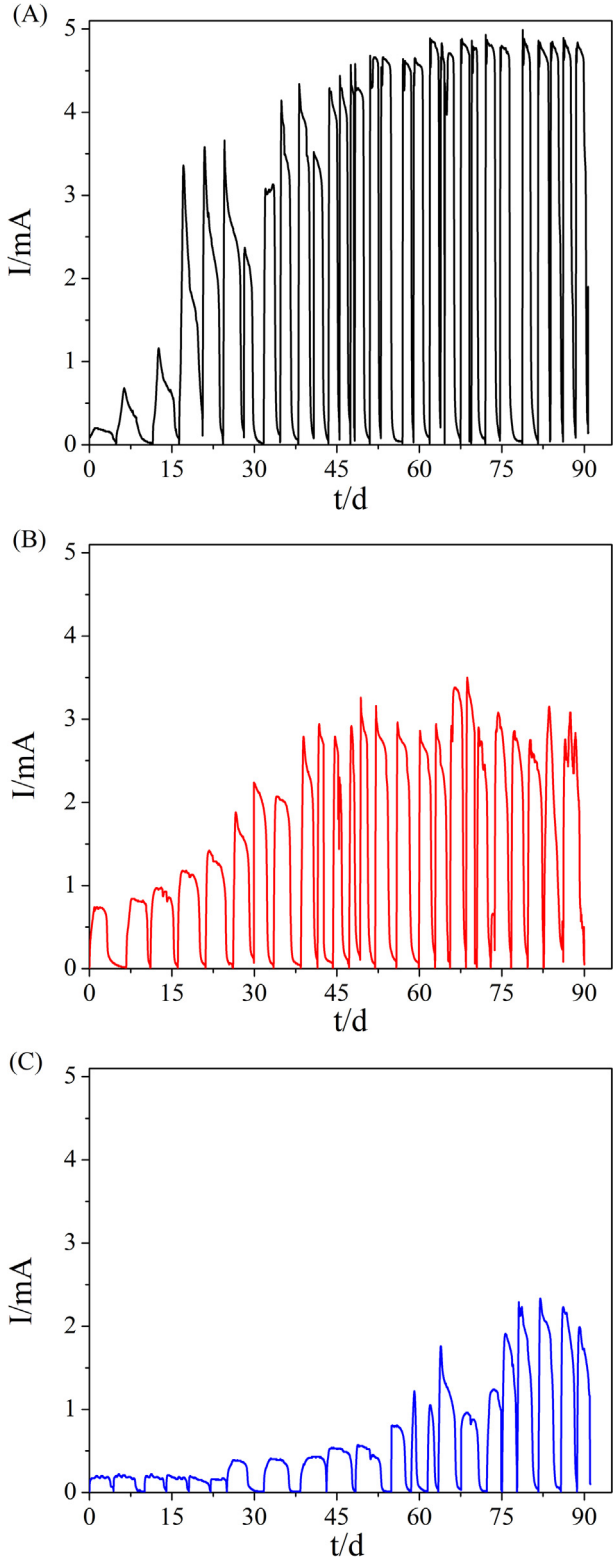

Fig. 1. Long-term bio-current outputs in the initial and stable operation phases: (A) control; (B) 0.1 mg L^{-1} chlorine; and (C) 0.5 mg L^{-1} chlorine.

the homogeneous growth of the electroactive bacteria on the anode. However, the startup time and maximum current output differed significantly. The BES-0 required an approximately 15 day activation and enrichment period to achieve an apparent current jump, while the BES-0.1 and BES-0.5 took at least 30 and 55 days to achieve a current jump, respectively (Fig. 1). A shorter startup time was associated with a higher current output of 4.9 ± 0.3 mA for BES-0, which was 1.5- and 2.2-fold higher than those of 3.2 ± 0.3 mA for BES-0.1 and 2.2 ± 0.5 mA for BES-0.5, respectively. The EABs under chronic chlorine exposure exhibited lower electroactivity with a longer cycle time of almost 4 days for both BES-0.1 and BES-0.5, compared with that of 2.5 days for BES-0, which was likely due to the slower acetate degradation resulting from lower electroactivity (Fig. 2A). The BES-0 also exhibited the highest power density of 0.5 ± 0.1 W m^{-2}, normalized to the CEM projected surface area (Fig. 2B). The current conversion efficiency of BES-0 was 46%, which was much higher than those of 33% for BES-0.1 and 27% for BES-0.5, indicating the deteriorative electroactivity of EABs after chronic chlorine exposure.

The mature EABs were further investigated for their response to chronic chlorine exposure by turnover and non-turnover CVs. All BESs exhibited similar sigmoidal waves for EABs in the turnover CVs, suggesting that the EABs followed a typical electron transfer model (Fig. 2C and 2D) [28]. The EAB current of BES-0 (5.1 ± 0.4 mA) demonstrated a higher electroactivity than those of BES-0.1 (3.6 ± 0.5 mA) and BES-0.5 (1.9 ± 0.3 mA). Turnover CV results were in accordance with the current output, demonstrating the metabolic activity reduction of the electroactive bacteria under chronic chlorine exposure. Non-turnover CVs at various scan rates were conducted to reveal the underlying electron transfer mechanisms and to indicate the controlled step in the electron transfer process (Fig. 3). When the scan rate was increased from 1 to 100 mV s^{-1}, the potentials shifted negatively and the peak current intensities increased. The peak current intensities of all anodes exhibited a linear correlation with the root square of the scan rate (scan $rate^{1/2}$), indicating that the diffusion processes controlled the electrochemical reaction [28]. Thus, the main mechanism of electron transfer pathway of EABs was more likely to be mediated electron transfer (MET). This electron transfer pathway was likely to be attributed to the thick EAB and mixed culture conditions, which was distinct to previous research where the EAB was generally composed of acetate-fed *Geobacter* sp. and exhibited a direct electron transfer pathway [29]. Mixed communities were generally involved in complex electrochemical reactions mediated by the electron transfer network inside the EPS. The distant electron transfer towards the electrode was closely associated with intercellular conductive substance. For example, some mediator carriers (e.g. phenazine and phenazine-1-carboxamide) produced by *Pseudomonas* sp. played a vital role in the electron transfer in EAB [30]. It was worth noting that the values of the slopes decreased from EAB-0 to EAB-0.5 (Table S2), indicating the spatial structure and composition of EPS might be adverse to MET in EAB-0.1 and EAB-0.5.

3.2. Distribution and composition of EPS in EABs

3.2.1. Distribution characteristics of EPSs in EABs

The EPS functions as biofilm skeleton to support its mechanical structure, and hence, the spatial structure of the EPS must be well constructed. The triple staining CLSM and SEM images

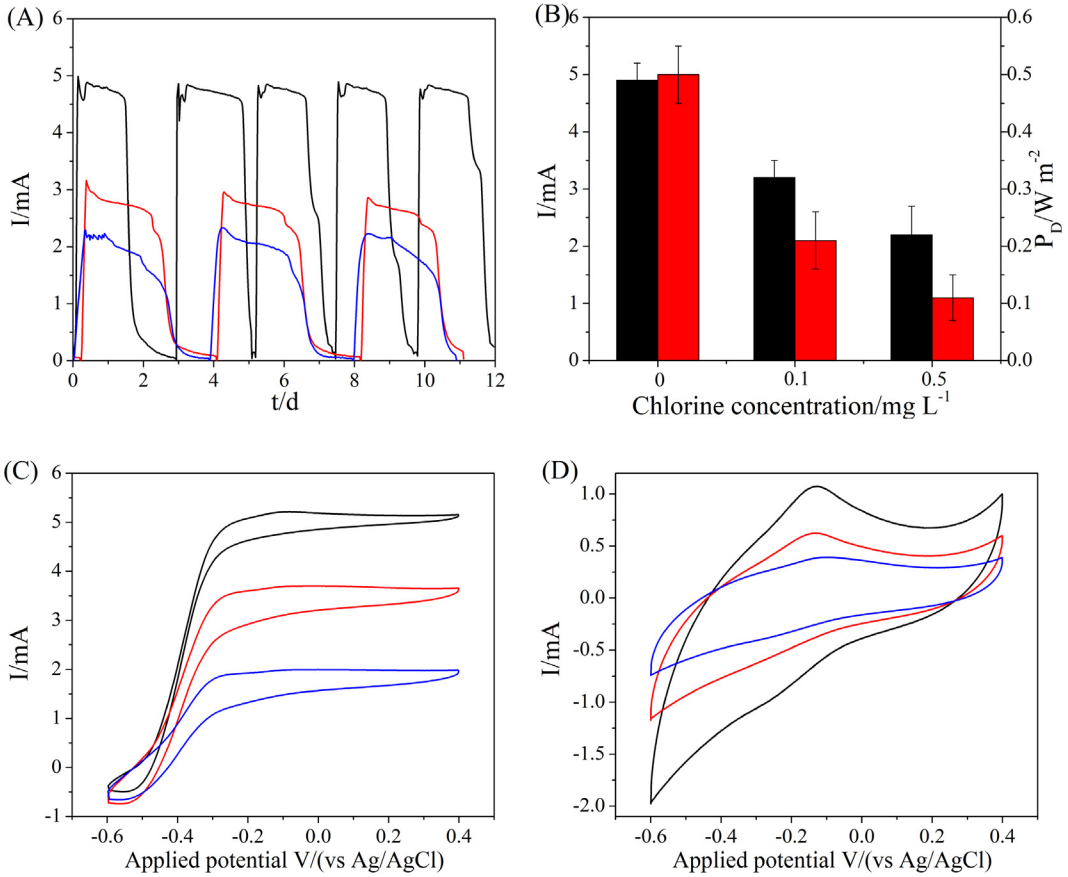

Fig. 2. (A) Current output versus time after inoculation (black line, BES-0; red line, BES-0.1; blue line, BES-0.5); (B) comparison of EAB current recovery and power density (black bar for current, and red bar for power density); (C) turnover and (D) non-turnover CV scans at 1 mV s^{-1} of EABs (black line, EAB-0; red line, EAB-0.1; blue line, EAB-0.5) under various chlorine exposure conditions.

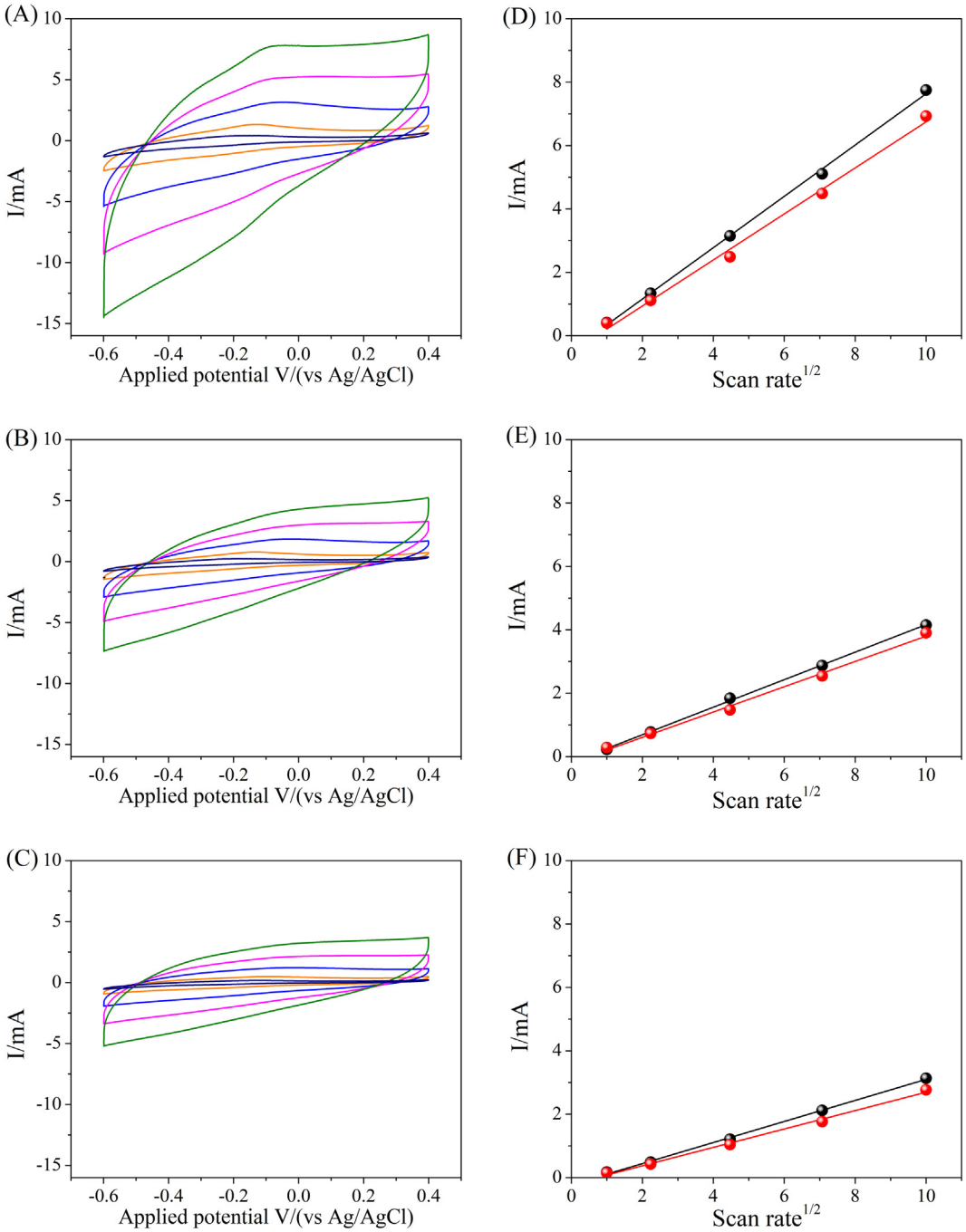

Fig. 3. Non-turnover CVs of EABs at different scan rates (navy, orange, blue, magenta, olive lines represented 1, 5, 20, 50, 100 mV s^{-1}), and linear relationship of peak current and square root scan rate: (A) and (D) control; (B) and (E) 0.1 mg/L chlorine; (C) and (F) 0.5 mg/L chlorine. The black and red points represented oxidation and reduction peak current, and the black and red lines represented the fitted curves (oxidation curves: R^2 = 99.8% for EAB-0, 99.8% for EAB-0.1, 99.7% for EAB-0.5; reduction curves: R^2 = 99.3% for EAB-0, 99.4% for EAB-0.1, 99.4% for EAB-0.5).

revealed that the EABs were morphologically heterogenous, with protein and α- and β-D-glucopyranose PS clearly detected (Fig. 4 and S1). The proteins were all observed in EAB-0, EAB-0.1, and EAB-0.5. The α-D-glucopyranose PS was dispersed in a single region of EAB-0 visual field, while it sharply dispersed to nearly the whole visual field in EAB-0.1, and subsequently returned to a comparative dispersion status with EAB-0 under the chlorine concentration of 0.5 mg L^{-1} (EAB-0.5). The β-D-glucopyranose PS was observed in a limited number of spots in EAB-0 and EAB-0.1, and was thus greatly surpassed by protein and α-D-glucopyranose PS in terms of visual observations. After the EAB was chronically exposed to 0.5 mg L^{-1} chlorine, the β-D-glucopyranose PS content dramatically increased and became the dominant component, suggesting its role as the principle protective barrier for high-concentration chlorine exposure. Besides, it also suggested the protective mechanisms of EPS on electroactive bacteria differed from that in EAB-0 or EAB-0.1. The increased contents of α- and β-D-glucopyranose PS implied that chlorine exposure could stimulate the secretion of massive PS significantly.

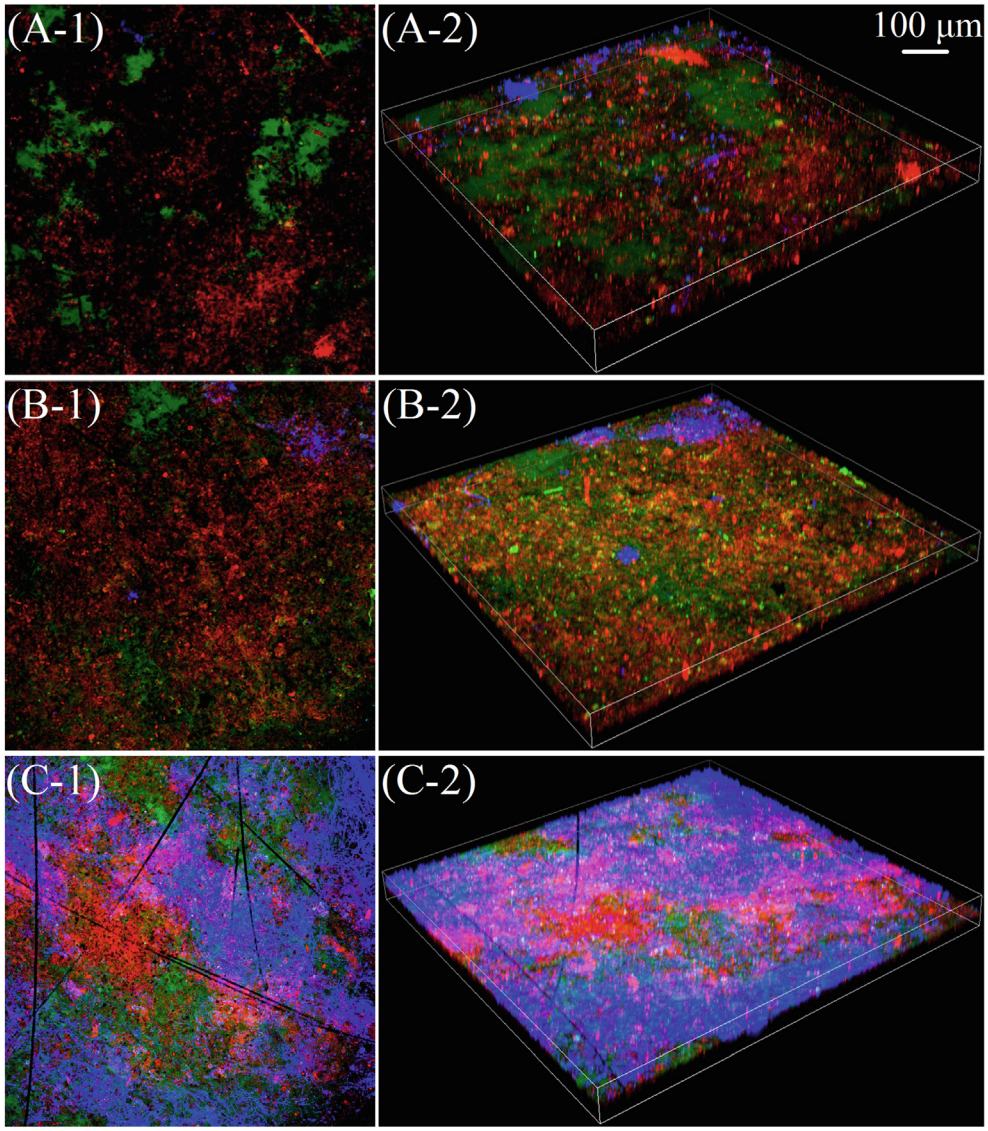

Fig. 4. Effects of chronic chlorine exposure on the EPS spatial distributions in the EABs. Left (right) column represents the 2D (3D) images of the brightest layer in each sample (A: control; B: 0.1 mg L^{-1} chlorine; and C: 0.5 mg L^{-1} chlorine). Biofilms were simultaneously stained with FITC (proteins in green), Con A (α-D-glucopyranose PS in red) and CW (β-D-glucopyranose PS in blue).

The semi-quantitative analysis of the 3D CLSM images was conducted to investigate the spatial distribution and relative content of protein and polysaccharides (Fig. 5). Close to the center of the vertical direction, the total pixel values of the 3 components increased exponentially from the bottom layer to the brightest layer, followed by a sharp reduction at the top layer, almost reaching zero. An EMG model was used to exhibit the distribution of each component, with relevant parameters listed in Table S3. The proteins were dispersed in the center of EAB-0 with a thickness approaching 60 μm, and narrowed to 50 μm and 45 μm for EAB-0.1 and EAB-0.5, respectively. Moreover, the peak intensities of the proteins were observed to significantly decrease with the chronic chlorine exposure. Low-concentration chlorine exposure (0.1 mg L^{-1}) significantly increased the production of α-D-glucopyranose PS, evidenced by the increased values of A (5.71×10^8) and w (10.39). Similar values of A and w for EPS-0 (A: 1.83×10^8, w: 7.88) and EPS-0.5 (A: 1.88×10^8, w: 7.85) indicated that the production of α-D-glucopyranose PS was not affected by the high-concentration chlorine exposure (0.5 mg L^{-1}). The x_c value of α-D-glucopyranose PS exhibited a reduction from 48.81 μm (EAB-0) to 33.63 μm (EAB-0.1), demonstrating a shift from the center to the surface of EAB. This might imply the role of α-D-glucopyranose PS as a protective component under low-concentration chlorine exposure. It was inferred that the increased production of α-D-glucopyranose PS under low-concentration chlorine exposure (0.1 mg L^{-1}) following by abrupt reduction under chlorine concentration of 0.5 mg L^{-1} was probably due to its low thermodynamic stability and poor dispersity [31–33]. The production of β-D-glucopyranose PS increased slightly in EAB-0.1, followed by a dramatic rise by 18.5 times that of EAB-0 after high-concentration chlorine exposure. The w value of EAB-0.5 at 9.78 μm, which was 45.3% higher than that of 6.73 μm for EAB-0, verified the maintaining of the biofilm due to the elevated production of β-D-glucopyranose PS. Furthermore, the x_c value of β-D-glucopyranose PS reduced from 45.11 μm (EAB-0) to 32.08 μm (EAB-0.5), indicating its ability to broaden the distribution width throughout the entire EAB skeleton. These results clearly identify the enhanced β-D-glucopyranose PS production as a protective response to chronic high-concentration chlorine exposure.

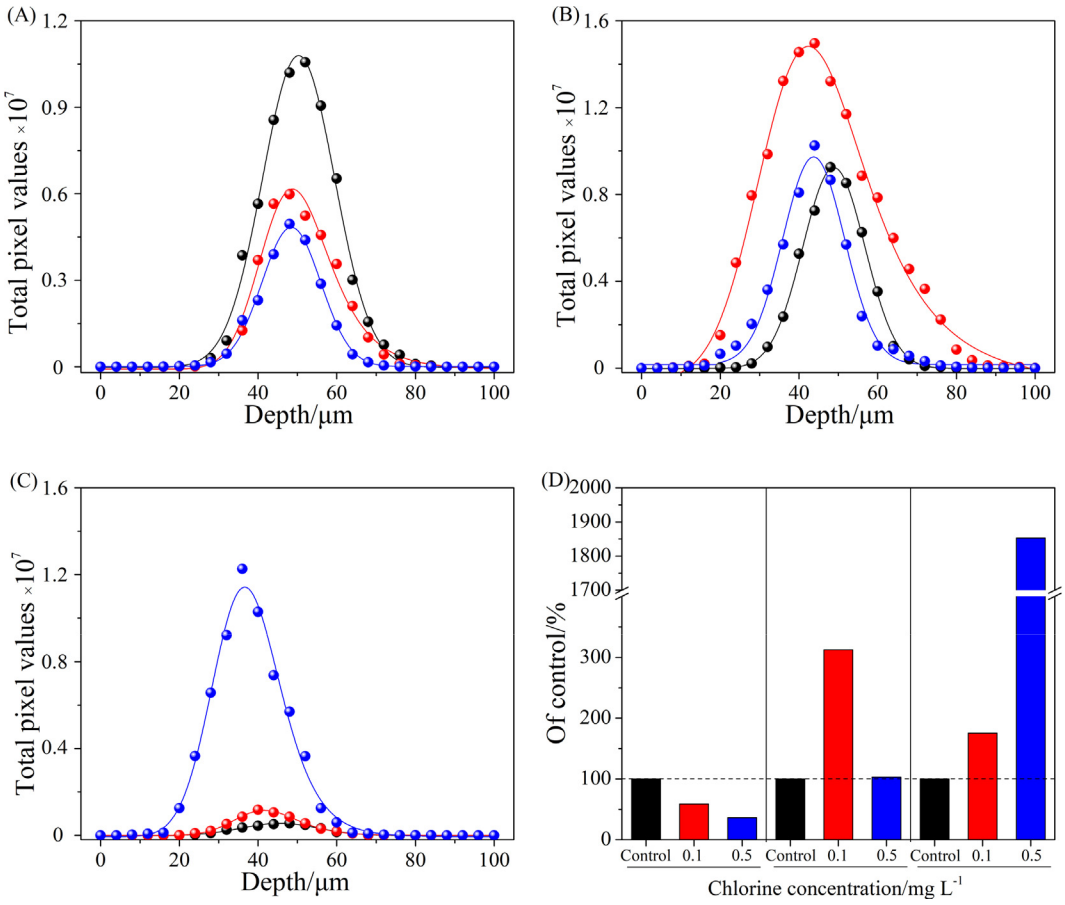

Fig. 5. Intensity distributions of (A) proteins, (B) α-D-glucopyranose PS, (C) β-D-glucopyranose PS in each layer (black line, EAB-0; red line, EAB-0.1; blue line, EAB-0.5); and (D) relative total content of protein (left region), α-D-glucopyranose PS (middle region) and β-D-glucopyranose PS (right region) in the EABs under various chlorine exposure conditions.

3.2.2. Composition characteristics of EPSs in EABs

The composition of EPS formed under different chlorine exposure conditions was analyzed (Fig. 6A). A total of 570 ± 14 mg EPS g^{-1} VSS was produced from EAB-0.5, which was 2.7- and 3.5-fold higher than those measured for EAB-0.1 (211 ± 14 mg EPS g^{-1} VSS) and EAB-0 (163 ± 10 mg EPS g^{-1} VSS), respectively. The EAB growing under the high-concentration chlorine exposure exhibited the highest EPS production, agreeing with the CLSM imaging results. The enhanced EPS production under external interference was also observed in the literature, demonstrating the improved bacterial adhesion, barrier formation, and energy storing of the EAB [34,35]. EPS was composed of TB-EPS and LB-EPS according to its adhesion state with bacterial cells. The relative proportion and content of TB-EPS and LB-EPS were a function of the various chlorine exposure conditions. The maximum EPS production was associated with a higher production of LB-EPS and TB-EPS in EAB-0.5. The yields determined for TB-EPS (356 ± 16, 127 ± 10, 92 ± 7 mg EPS g^{-1} VSS) were higher than those of LB-EPS (214 ± 15, 84 ± 7, 71 ± 6 mg EPS g^{-1} VSS) for EAB-0.5, EAB-0.1, and EAB-0, respectively. The LB-EPS/TB-EPS ratio of 77% was determined in the absence of chlorine exposure, which was higher than that observed for EAB-0.1 and EAB-0.5. This demonstrated that chronic chlorine exposure accelerated the secretion of both LB-EPS and TB-EPS, while TB-EPS played a more important role in protecting the EABs than LB-EPS.

Both proteins and PS were homogenously distributed in the EAB. The total protein contents were observed as 101 ± 7, 85 ± 4, 72 ± 5 mg g^{-1} VSS for EAB-0, EAB-0.1, EAB-0.5 respectively, with corresponding total PS contents of 62 ± 4, 136 ± 5, 498 ± 12 mg g^{-1} VSS. This indicated PS as the predominant EPS component under chronic chlorine exposure. The protein content gradually decreased from 46 ± 3 to 19 ± 1 mg g^{-1} VSS in LB-EPS, while for TB-EPS it was maintained relatively stable at approximately 50 mg g^{-1} VSS. The PS contents in LB-EPS and TB-EPS were observed to increase significantly from 25 ± 2 to 196 ± 10 mg g^{-1} VSS and from 37 ± 1 to 303 ± 6 mg g^{-1} VSS, respectively, with the increased dosage of chlorine (Fig. 6B and 6C). The enhanced PS component in both LB-EPS and TB-EPS acted as a thicker protective barrier for the electroactive bacteria under chlorine exposure. The preferential presence of extracellular PS was also reported in previous research under environmental stress, where accumulation of PS on the cell-electrode interface induced by various anode potential [36].

3.3. Microbial properties of EABs

The EAB-0 exhibited the highest biomass adhesion ratio (k_b) of 0.33 ± 0.02 mg VSS mg^{-1} carbon fiber, which was higher than that of 0.26 ± 0.02 mg VSS mg^{-1} carbon fiber for EAB-0.5 ($p < 0.05$, Student's *t*-test, Table S4), but similar to 0.28 ± 0.03 mg VSS mg^{-1} carbon fiber for EAB-0.1. However, no statistically significant differences were observed between the protein adhesion ratios (k_p) of EAB-0, EAB-0.1, and EAB-0.5 (0.13 ± 0.03, 0.12 ± 0.02, 0.11 ± 0.02 mg protein mg^{-1} carbon fiber, respectively) (Fig. 7A). The biofilm electroactivity (BE) was closely associated with the current generation performance of the EABs. The similar protein

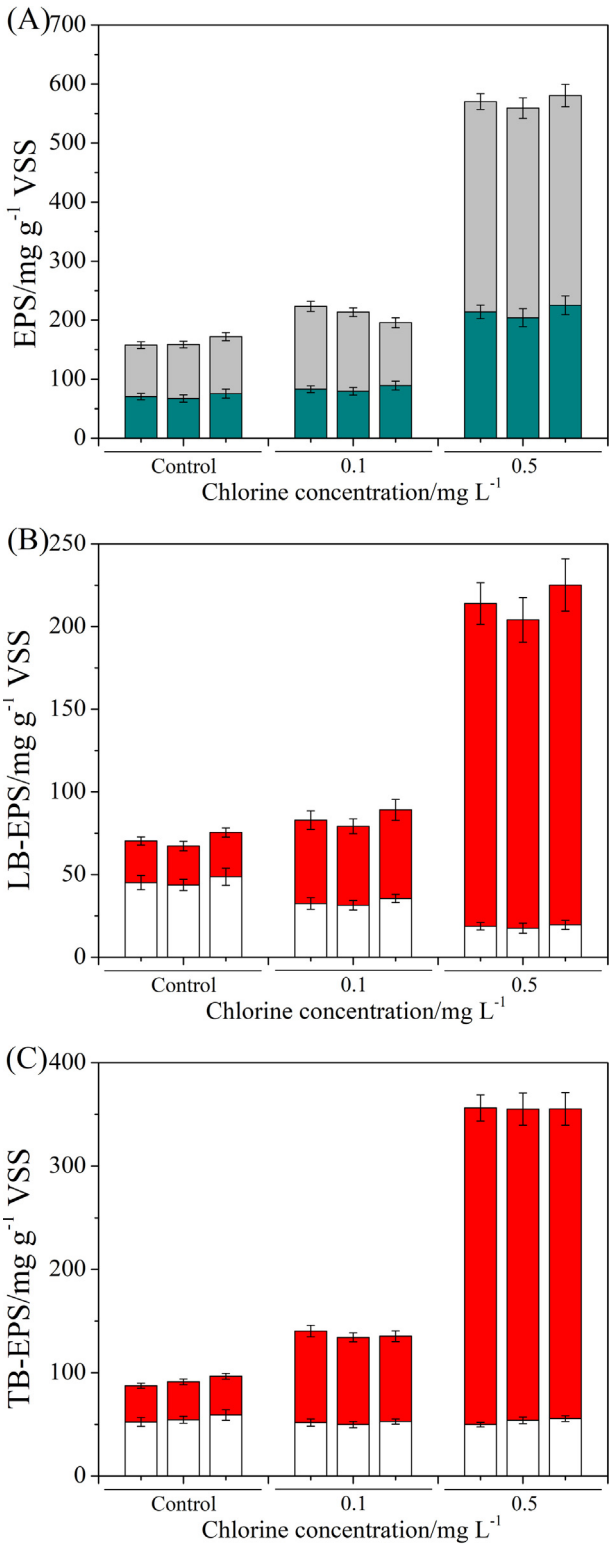

Fig. 6. (A) TB-EPS and LB-EPS contents of the EABs (gray and cyan bars for TB-EPS and LB-EPS), and protein and PS concentrations in the EPSs under various chlorine exposure conditions: (B) LB-EPS and (C) TB-EPS, respectively (red and white bars for PS and protein).

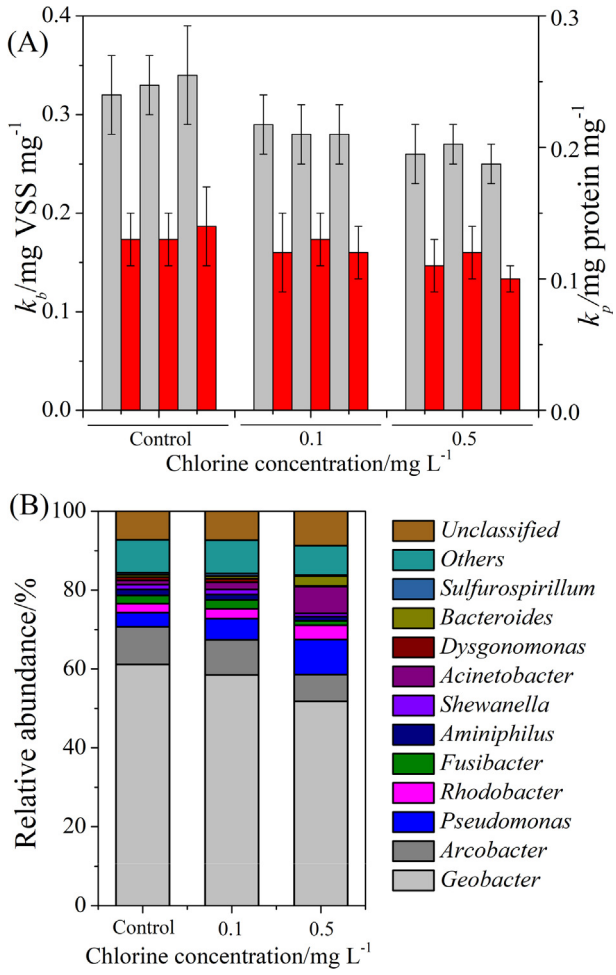

Fig. 7. (A) Biomass adhesion ratio (k_b, gray bar) and protein adhesion ratio (k_p, red bar); and (B) microbial communities of EABs under various chlorine exposure conditions.

adhesion ratios did not exhibit the same level of electroactivity. In particular, the BE dropped to 6.5 ± 0.8 mA g^{-1} protein (EAB-0.1) and 5.1 ± 0.5 mA g^{-1} protein (EAB-0.5) after chronic chlorine exposure, both of which were much lower than 9.3 ± 0.7 mA g^{-1} protein for EAB-0 (Fig. S2). This suggested that a major portion of the protein components in the EAB under chronic chlorine exposure was poorly correlated with the electron transfer process. Previous research demonstrated the crucial role of several enzymes in maintaining the relative stability of the EPS contents, such as β-N-acetylhexosaminidase (NAG, related to the hydrolysis of PS) and leucyl aminopeptidase (LAP, related to the degradation of Protein) [37,38]. The corresponding protein synthesis system could be activated by stimulation of high-concentration EPS. Despite serving as a protective barrier against the chlorine, EPS could also prevent the nutrients from penetrating into the core EAB layer. Then, the excessive EPS might be degraded into bioavailable substrate by these enzymes for inner electroactive bacteria [39,40]. This subsequently increased the EPS protein production while having a reduced contribution to the electron transfer.

Chronic chlorine exposure also imposed external pressure on the formation of bacterial communities. A total of 353 OTUs were shared among all EABs, while 31, 26, and 23 OTUs were unique to EAB-0, EAB-0.1, and EAB-0.5, respectively (Fig. S3). *Geobacter*, known as a model genus of exoelectrogens, was preferentially enriched in all EABs, as observed for other acetate-fed BESs (Fig. 7B) [29]. Its relative abundance gradually decreased from 61% in EAB-0 to 52% in EAB-0.5, revealing the suppression of *Geobacter* under chronic chlorine exposure. A reduction in *Arcobacter* was also observed (from 10% to 7%), which was in accordance with the BE results. This suggested that the EAB electroactivity

was synergistically modulated by *Arcobacter*, which was as reported to promote electron transfer in an acetate-fed BES [41]. Conversely, *Acinetobacter* was enhanced from 1% to 2%, reaching 7% with the gradual addition of chlorine. The cell membrane of *Acinetobacter* was highly hydrophobic and could secret excess EPS [42]. The increased abundance of *Acinetobacter* may be attributed to the chronic adaptation to chlorine. Moreover, the *Pseudomonas* genus was also observed to be highly enriched in EAB-0.5, with the relative abundance of 9%. This was significantly higher than those of 5% and 4% for EAB-0.1 and EAB-0, respectively. *Pseudomonas*, closely related to PS secretion in biofilm, facilitated the supporting function of the biofilm structure [43,44]. It was inferred that *Pseudomonas* played an important role in regulating the production of EPS, acting as a physical barrier to weaken the toxicity of the chlorine.

3.4. Discussion

The relationships between electricity generation performance and concentration of EPS components were quantified using Pearson correlation analysis in order to identify the main factors governing EAB electroactivity (Table S5). Among the parameters, the current output demonstrated a strong positive correlation with EAB electroactivity ($r = 0.978$, $P < 0.01$) and k_b ($r = 0.946$, $P < 0.01$), as expected. A high correlation was also identified between current output and the total protein content in EPS ($r = 0.928$, $P < 0.01$), indicating the function of the total EPS protein as a conductive matrix for electron transfer in EAB. In particular, the current output was weakly correlated with the TB-EPS protein ($r = 0.334$), while a significant correlation ($r = 0.854$, $P < 0.01$) was determined between current output and the LB-EPS protein content. This may be attributed to the potential initial interaction between the chlorine and the out-layer LB-EPS, inactivating and decomposing the active proteins in the LB-EPS by the extracellular enzymes. This consequently gradually decreased the LB-EPS protein content. The inner-layer protein content of the TB-EPS was maintained at stable level, probably because: (1) The inner-layer protein played a more prominent role in electroactive bacteria adhesion on the electrode surface; and (2) the outer-layer LB-EPS, acting as a physical barrier for the TB-EPS, reduced the impact of the chronic chlorine exposure on the inner-layer protein. Conversely, strong negative correlations were observed between the current output and the PS contents in both TB-EPS ($r = -0.860$, $P < 0.01$) and LB-EPS ($r = -0.839$, $P < 0.01$). The extracellular PS served as a biofilm skeleton to shape the EAB under the disinfection system, and exhibited a relatively high adsorption capacity by binding with the chlorine. However, the over secretion of nonconductive PS obstructed the electron transfer between the redox-active proteins and the electrode, which may have been a direct attributor to the low electroactivity of EAB-0.1 and EAB-0.5.

The pollutant removal performance was the primary function of EAB. The response variation of EAB to substrate was monitored in order to evaluate the effect of chronic chlorine exposure on the pollutant removal (Fig. 8A and 8B). There was an obvious positive correlation between $-k_{COD}$ and current output ($r = 0.958$, $P < 0.01$), suggesting the substrate degradation in BES was still regulated by the electrochemical process in the presence of chlorine. Previous studies have reported that acetate degradation could be

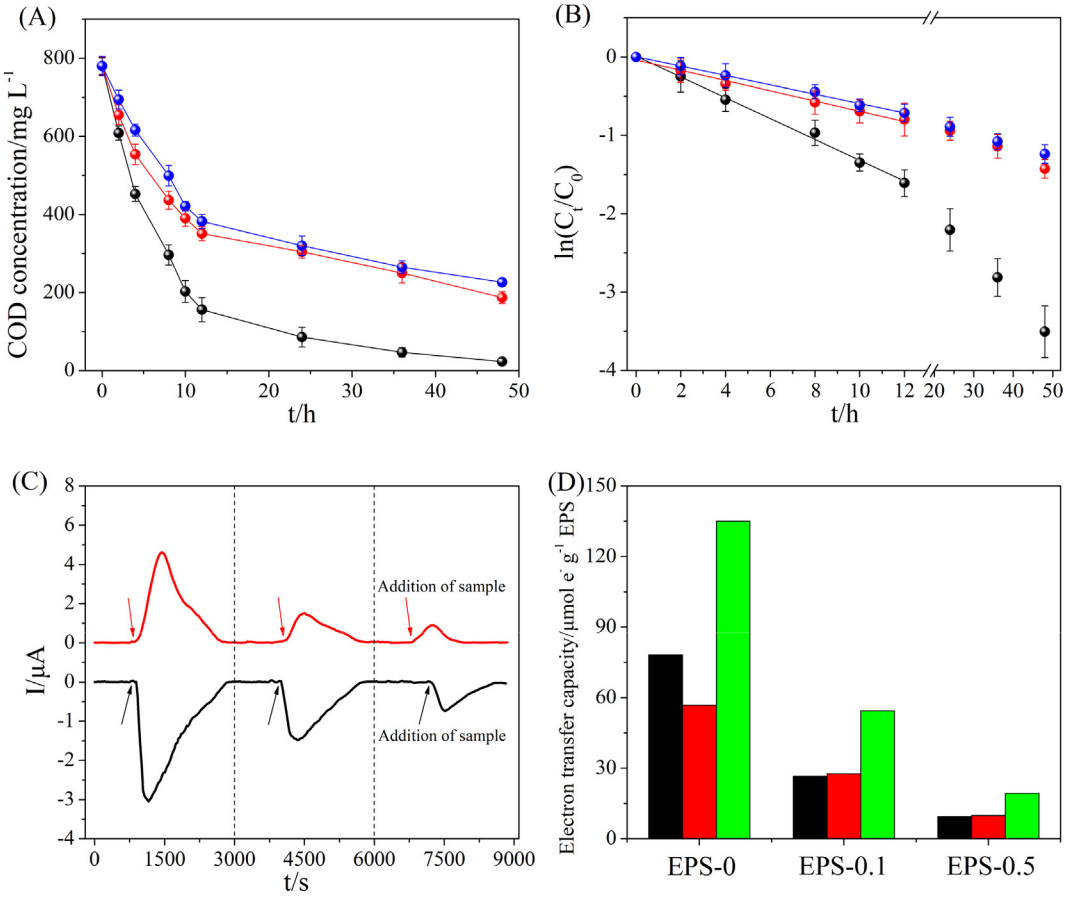

Fig. 8. (A) Pollutant degradation rate within 48 h (black line, EAB-0; red line, EAB-0.1; blue line, EAB-0.5), and (B) first-order degradation kinetics (EAB-0, $R^2 = 99.4\%$, $k = -0.133$; EAB-0.1, $R^2 = 98.9\%$, $k = -0.065$; EAB-0.5, $R^2 = 99.5\%$, $k = -0.059$) in the first 12 h of EABs under various chlorine exposure conditions; (C) reductive and oxidative current responses of EPSs (left region, EAB-0; middle region, EAB-0.1; right region, EAB-0.5); (D) electron transfer capacity of EPSs (black, red, and green bars for EAC, EDC, and EEC).

described by a first-order saturated equation [45], which was also observed in this chlorine-interfered BES. The first-order degradation rate constant ($-k_{COD}$) for EAB-0 was determined as 0.133 h^{-1}, which was 2.3-fold higher than that of 0.059 h^{-1} for EAB-0.5, indicating the inhibition of EAB electroactivity under chronic chlorine exposure. Besides microbial composition, the current generation performance in thick EAB was also heavily dependent on capacity of EPS to transfer electrons. The MEO results returned EDCs of 56.9, 27.7, and 9.8 μmol e^- g^{-1} EPS for EPS-0, EPS-0.1, and EPS-0.5. Correspondingly, the maximum EAC was found in the EPS-0 (78.2 μmol e^- g^{-1} EPS), followed by the EPS-0.1 (26.7 μmol e^- g^{-1} EPS), and the EPS-0.5 (9.5 μmol e^- g^{-1} EPS). The EEC of EPS-0 (135.1 μmol e^- g^{-1} EPS) was significantly higher than those of EPS-0.1 (54.4 μmol e^- g^{-1} EPS) and EPS-0.5 (19.3 μmol e^- g^{-1} EPS) (Fig. 8C and 8D). The high EEC of EPS-0 reflected the excellent electron transfer capability, which was capable of assisting distant bio-electron transfer, consequently facilitating substrate degradation.

Essentially, chronic chlorine exposure was determined to exert a great impact on the formation on EAB and its electrochemical performance. EPS yields were synergistically regulated by the bacteria as a self-protection mechanism, resulting in a loss in extracellular electron transfer. However, the functional genes associated with the production and transport of the major components of EPS including polysaccharides, adhesion proteins, and pili proteins should be further studied (detailed information the SI).

4. Conclusion

This study proved that EAB electroactivity could be deteriorated after chronic chlorine exposure. The main reason for this deterioration was an enhanced production and broader distribution of α-D-glucopyranose PS in EAB-0.1 and β-D-glucopyranose PS in EAB-0.5, while the protein contents decreased significantly. This microbial response to chronic chlorine exposure also limited the current-regulated pollutant degradation efficiency. Further studies are needed to investigate the performance variation of engineered EAB with extensive use of chlorine disinfectant in wastewater by taking the hydraulic scouring effect into consideration.

CRediT authorship contribution statement

Yue Dong: Data acquisition, Data analysis and Interpretation, final approval of the submitted version. **Mingrui Sui:** Study conception and design, data acquisition, data analysis and interpretation, article critical revision, final approval of the submitted version. **Xin Wang:** Article drafting, article critical revision, final approval of the submitted version. **Peng Zhang:** Data analysis and interpretation, article critical revision, final approval of the submitted version. **Yiying Jiang:** Study conception and design, data analysis and interpretation, article drafting, article critical revision, final approval of the submitted version. **Jianyu Wu:** Study conception and design, data analysis and interpretation, article drafting, article critical revision, final approval of the submitted version.

Declaration of Competing Interest

The authors declare the following financial interests/personal relationships which may be considered as potential competing interests: The authors have consulted the Guide for Authors in preparing this submitted manuscript. The authors also confirm that the manuscript has been prepared in compliance with the Ethics in Publishing Policy as described in the Guide for Authors. The present publication is approved by all authors and tacitly or explicitly by the responsible authorities where the work is carried out. This submission also implies that, if accepted, it will not be published elsewhere in the same form, in English or in any other language, without the written consent of the publisher.

Acknowledgements

This work was supported by National Natural Science Fund of China (Grant No. 51909067 and Grant No. 51909065) and the Fundamental Research Funds for the Central Universities of China (Grant No. 2018B06514 and Grant No. B200202108).

Appendix A. Supplementary data

Supplementary data to this article can be found online at https://doi.org/10.1016/j.bioelechem.2021.107894.

References:

[1] H.M.K. Delanka-Pedige, S.P. Munasinghe-Arachchige, Y. Zhang, N. Nirmalakhandan, Bacteria and virus reduction in secondary treatment: Potential for minimizing post disinfectant demand, Water Res. 177 (2020) 1–6.
[2] J. Wang, J. Shen, D. Ye, X. Yan, Y.J. Zhang, W.J. Yang, X.W. Li, J.Q. Wang, L.B. Zhang, L.J. Pan, Disinfection technology of hospital wastes and wastewater: Suggestions for disinfection strategy during coronavirus Disease 2019 (COVID-19) pandemic in China, Environ. Pollut. 262 (2020) 1–10.
[3] H. Zhang, W.Z. Tang, Y.S. Chen, W. Yin, Disinfection threatens aquatic ecosystems, Science 368 (2020) 146–147.
[4] A.P. Borole, G. Reguera, B. Ringeisen, Z.W. Wang, Y. Feng, B.H. Kim, Electroactive biofilms: current status and future research needs, Energy Environ. Sci. 4 (2011) 4813–4834.
[5] X. Li, S. Chen, J. Zeng, K. Chabi, W.J. Song, X.X. Xian, X. Yu, Impact of chlorination on cell inactivation, toxin release and degradation of cyanobacteria of development and maintenance stage, Chem. Eng. J. 397 (2020) 1–10.
[6] R. Hou, C. Luo, S.F. Zhou, Y. Wang, Y. Yuan, S.G. Zhou, Anode potential-dependent protection of electroactive biofilms against metal ion shock via regulating extracellular polymeric substances, Water Res. 178 (2020) 1–9.
[7] B.E. Logan, J.M. Regan, Electricity-producing bacterial communities in microbial fuel cells, Trends Microbiol. 14 (2006) 512–518.
[8] G.P. Sheng, H.Q. Yu, X.Y. Li, Extracellular polymeric substances (EPS) of microbial aggregates in biological wastewater treatment systems: A review, Biotechnol. Adv. 28 (2010) 882–894.
[9] T.S. Magnuson, How the xap locus put electrical "Zap" in Geobacter sulfurreducens biofilms, J. Bacteriol. 193 (2011) 1021–1022.
[10] J.B. Rollefson, C.S. Stephen, M. Tien, D.R. Bond, Identification of an extracellular polysaccharide network essential for cytochrome anchoring and biofilm formation in Geobacter sulfurreducens, J. Bacteriol. 193 (2011) 1023–1033.
[11] S. Seeliger, R. Cord-Ruwisch, B. Schink, A periplasmic and extracellular c-type cytochrome of Geobacter sulfurreducens acts as a ferric iron reductase and as an electron carrier to other acceptors or to partner bacteria, J. Bacteriol. 180 (1998) 3686–3691.
[12] M. Kitayama, R. Koga, T. Kasai, A. Kouzuma, K. Watanabe, Structures, compositions, and activities of live Shewanella biofilms formed on graphite electrodes in electrochemical flow cells, Appl. Environ. Microb. 83 (2017) 1–11.
[13] Y.J. Feng, Q. Yang, X. Wang, B.E. Logan, Treatment of carbon fiber brush anodes for improving power generation in air-cathode microbial fuel cells, J. Power Sources 195 (2010) 1841–1844.
[14] T. Li, X. Wang, L. Zhou, J. An, J. Li, N. Li, H. Sun, Q. Zhou, Bioelectrochemical sensor using living biofilm to in situ evaluate flocculant toxicity, ACS Sensors 1 (2016) 1374–1379.
[15] B. Frolund, R. Palmgren, K. Keiding, P.H. Nielsen, Extraction of extracellular polymers from activated sludge using a cation exchange resin, Water Res. 30 (1996) 1749–1758.
[16] M. Aeschbacher, M. Sander, R.P. Schwarzenbach, Novel electrochemical approach to assess the redox properties of humic substances, Environ. Sci. Technol. 44 (2010) 87–93.
[17] F. Ye, Y. Ye, Y. Li, Effect of C/N ratio on extracellular polymeric substances (EPS) and physicochemical properties of activated sludge flocs, J. Hazard. Mater. 188 (2011) 37–43.
[18] X. Li, X. Wang, Y. Zhang, N. Ding, Q. Zhou, Opening size optimization of metal matrix in rolling-pressed activated carbon air–cathode for microbial fuel cells, Appl. Energ. 123 (2014) 13–18.
[19] M.-Y. Chen, D.-J. Lee, Z. Yang, X.F. Peng, J.Y. Lai, Fluorecent staining for study of extracellular polymeric substances in membrane biofouling layers, Environ. Sci. Technol. 40 (2006) 6642–6646.
[20] L. Li, Z. Dong, J. Lu, J. Dai, Q. Huang, C.-C. Chang, T. Wu, AN H.264/AVC HDTV watermarking algorithm robust to camcorder recording, J. Vis. Commun. Image R 26 (2015) 1–8.

[21] M.Y. Chen, D.J. Lee, J.H. Tay, K.Y. Show, Staining of extracellular polymeric substances and cells in bioaggregates, Appl. Microbiol. Biot. 75 (2007) 467–474.
[22] S.S. Adav, J.C.-T. Lin, Z. Yang, C.G. Whiteley, D.-J. Lee, X.-F. Peng, Z.-P. Zhang, Stereological assessment of extracellular polymeric substances, exo-enzymes, and specific bacterial strains in bioaggregates using fluorescence experiments, Biotechnol. Adv. 28 (2010) 255–280.
[23] G. You, P. Wang, J. Hou, C. Wang, Y. Xu, L. Miao, B. Lv, Y. Yang, Z. Liu, F. Zhang, Insights into the short-term effects of CeO2 nanoparticles on sludge dewatering and related mechanism, Water Res. 118 (2017) 93–103.
[24] G. Larsson, M. Törnkvist, Rapid sampling, cell inactivation and evaluation of low extracellular glucose concentrations during fed-batch cultivation, J. Biotechnol. 49 (1996) 69–82.
[25] APHA, Standard methods for examination of water and wastewater, American Public Health Association, Water Environment Federation, Washington, DC., 2005.
[26] D.D. Liang, W.H. He, C. Li, Y.L. Yu, Z.H. Zhang, N.Q. Ren, Y.J. Feng, Bidirectional electron transfer biofilm assisted complete bioelectrochemical denitrification process, Chem. Eng. J. 375 (2019) 1–10.
[27] E. Grushka, Characterization of exponentially modified Gaussian peaks in chromatography, Anal. Chem. 44 (1972) 1733–1738.
[28] K. Fricke, F. Harnisch, U. Schroder, On the use of cyclic voltammetry for the study of anodic electron transfer in microbial fuel cells, Energy Environ. Sci. 1 (2008) 144–147.
[29] Q. Du, Q. Mu, T. Cheng, N. Li, X. Wang, Real-time imaging revealed that exoelectrogens from wastewater are selected at the center of a gradient electric field, Environ. Sci. Technol. 52 (2018) 8939–8946.
[30] Y. Wang, S.E. Kern, D.K. Newman, Endogenous phenazine antibiotics promote anaerobic survival of Pseudomonas aeruginosa via extracellular electron transfer, J. Bacteriol. 192 (2010) 365–369.
[31] N.V. Joshi, V.S.R. Rao, Flexibility of the pyranose ring in α- and β-D-glucoses, Biopolymers. 18 (1979) 2993–3004.
[32] J.W. Brady, Molecular dynamics simulations of α-D-glucose, J. Am. Chem. Soc. 108 (1986) 8153–8160.
[33] J.W. Brady, Molecular dynamics simulations of β-D-glucopyranose, Carbohydr. Res. 165 (1987) 306–312.
[34] S.S. Adav, D.-J. Lee, J.-H. Tay, Extracellular polymeric substances and structural stability of aerobic granule, Water Res. 42 (2008) 1644–1650.
[35] B. Vu, M. Chen, R.J. Crawford, E.P. Ivanova, Bacterial extracellular polysaccharides involved in biofilm formation, Molecules 14 (2009) 2535–2554.
[36] G.Q. Yang, L.Y. Huang, Z. Yu, X.M. Liu, S.S. Chen, J.X. Zeng, S.G. Zhou, L. Zhuang, Anode potentials regulate Geobacter biofilms: New insights from the composition and spatial structure of extracellular polymeric substances, Water Res. 159 (2019) 294–301.
[37] Z. Chen, W. Zhang, D. Wang, T. Ma, R. Bai, Enhancement of activated sludge dewatering performance by combined composite enzymatic lysis and chemical re-flocculation with inorganic coagulants: Kinetics of enzymatic reaction and re-flocculation morphology, Water Res. 83 (2015) 367–376.
[38] J. Habermacher, A.D. Benetti, N. Derlon, E. Morgenroth, The effect of different aeration conditions in activated sludge-Side-stream system on sludge production, sludge degradation rates, active biomass and extracellular polymeric substances, Water Res. 85 (2015) 46–56.
[39] S. Huang, N. Voutchkov, S. Jiang, Balancing carbon, nitrogen and phosphorus concentration in seawater as a strategy to prevent accelerated membrane biofouling, Water Res. 165 (2019) 114978.
[40] F. Ye, G. Peng, Y. Li, Influences of influent carbon source on extracellular polymeric substances (EPS) and physicochemical properties of activated sludge, Chemosphere 84 (2011) 1250–1255.
[41] S.L. Li, K.H. Nealson, Enriching distinctive microbial communities from marine sediments via an electrochemical-sulfide-oxidizing process on carbon electrodes, Front. Microbiol. 6 (2015) 1–8.
[42] Y. Lv, C. Wan, D.J. Lee, X. Liu, J.H. Tay, Microbial communities of aerobic granules: Granulation mechanisms, Bioresour. Technol. 169 (2014) 344–351.
[43] J.D. Shrout, R. Nerenberg, Monitoring bacterial twitter: Does quorum sensing determine the behavior of water and wastewater treatment biofilms, Environ. Sci. Technol. 46 (2012) 1995–2005.
[44] Y. Sakuragi, R. Kolter, Quorum-sensing regulation of the biofilm matrix genes (pel) of Pseudomonas aeruginosa, J. Bacteriol. 189 (2007) 5383–5386.
[45] G.S. Jadhav, M.M. Ghangrekar, Performance of microbial fuel cell subjected to variation in pH, temperature, external load and substrate concentration, Bioresour. Technol. 100 (2009) 717–723.